NASA TECHNICAL TRANSLATION NASA TT F-12,602

NASA TT F-12,602

CALCULATION OF THE MOTION OF A SHOCK WAVE AND FLOW PARAMETERS IN A SHOCK TUBE WITH A NONINSTANTANEOUSLY OPENING DIAPHRAGM

Zh.S. Duntsova, I.V. Yershov, V.T. Kireyev, and Ye.I. Ruzavin

Translation of
"Raschet dvizheniya udarnoy volny i parametrov potoka pri nemgnovennom otkrytii diafragmy v udarnoy trube."

In: Izvestiya Akademii Nauk SSSR, Mekhanika zhidkosti i gaza, No. 2, pp. 102-128, March-April 1969

NATIONAL AERONAUTICS AND SPACE ADMINISTRATION
WASHINGTON, D.C. 20546 JULY 1970

NASA TT F-12,602

CALCULATION OF THE MOTION OF A SHOCK WAVE AND FLOW PARAMETERS IN A SHOCK TUBE WITH A NONINSTANTANEOUSLY OPENING DIAPHRAGM /120*

Zh.S. Duntsova, I.V. Yershov, V.T. Kireyev, and Ye.I. Ruzavin
(Moscow)

ABSTRACT: Calculation of changes in the shock-wave velocity and gas-flow parameters in the process of noninstantaneous opening of the diaphragm of a shock tube. The method of characteristics is used in developing the computer algorithms applied in the calculations. The calculated values for shock-wave velocities and gas-flow parameters are compared with experimental results for a number of steel, aluminum, and brass diaphragms of various designs.

Calculated results are presented for the variation of shock-wave propagation velocity on opening of the diaphragm and the parameters of the driving and driven gases on the accelerating section of a single-diaphragm shock tube. The computed values are compared in some cases with values measured experimentally.

It is known that the basic factor determining the deviation of flow stereotype from that predicted from the ideal theory [1, 2] on the initial path of shock-wave motion in a shock tube is the fact that the diaphragm does not open instantaneously [1-3]. Noninstantaneous diaphragm opening results in acceleration of the shock wave on an accelerating segment [1-3], the presence of nonunidimensional flow in the vicinity of the diaphragm [2, 4, 5], the experimentally observed density nonuniformity of the driven gas [6], and an increase in the maximum shock-wave velocity over that of the ideal theory [3]. Reference [3] proposes a calculation model that enables us to take into consideration only the increase in the maximum shock-

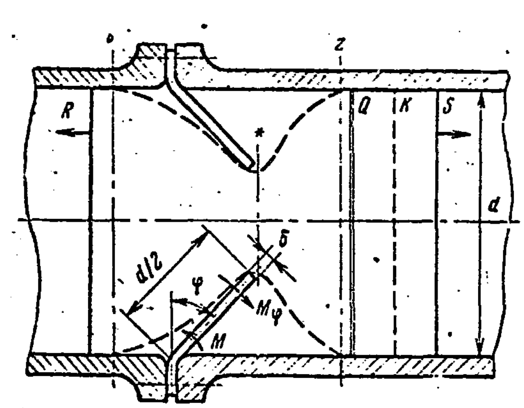

Figure 1

*Numbers in the margin indicate pagination in the foreign text.

wave velocity over the length of the tube among all of the deviations from the ideal shock-tube model indicated above. The flow model proposed in [7], which was used in the present study, permits determination of the mode of opening of the diaphragm and the associated variations in shock-wave velocity and the flow variables of the driving and driven gases.

1. A three-dimensional nonsteady flow that is very difficult to calculate numerically arises around the diaphragm as it opens. In the flow schematization used here [7], which is represented in Fig. 1, it is assumed that the gas in the high-pressure chamber expands in a one-dimensional nonsteady decompression wave R and that the variables of the gas passing across this wave in section 1, in the critical section *, and in section z (in which the expanding jet of driving gas reaches the chamber walls) are interrelated at any point in time by the equations of one-dimensional steady flow (quasistationary flow).

If we assume that the flow on the quasistationary segment is isentropic, the equation system connecting the driving-gas variables from the initial sections to section z, in combination with the law of variation of flow-section area $f_* = f_*(t)$ at time t, enables us to determine the supersonic-flow variables in section z as functions of time. Obviously, the variation of the latter determines the subsequent flow, which we shall assume to be one-dimensional and nonsteady. Here, as in [3], reflection of the flow from the tube walls is not taken into account.

The coordinate of the section in which the diaphragm is mounted is taken as the approximate coordinate x of section z, since, according to [4], the segment with essentially two-dimensional flow near the diaphragm is much smaller than the total acceleration distance. /121

In [7], the relationship $f_* = f_*(t)$ was found by simultaneous solution of the equations

$$t = t_0 + \int_{\varphi_0}^{\varphi} \frac{d\varphi}{\Phi(\varphi)}, \qquad \Phi(\varphi) = \left[\frac{2}{J}\int_{\varphi_0}^{\varphi}(M_\varphi - M)\,d\varphi + \dot{\varphi}_0^2\right]^{1/2} \tag{1.1}$$

which were obtained by integrating the equations

$$\ddot{\varphi} = \frac{1}{J}[M_\varphi - M], \qquad \frac{f_*}{f_-} = 1 - \cos\varphi \tag{1.2}$$

Here, ϕ is the blade rotation angle, $\dot{\phi}_0$ and ϕ_0 are the angular velocity and rotation angle of the blade at time t_0, I is the moment of inertia, M_ϕ is the torque, M is the moment of resistance, and f_- is the cross-sectional area of the low-pressure chamber. (Here and below, the subscripts minus and plus denote variables in the low- and high-pressure chambers, respectively.) The opening time of the diaphragm depends only slightly on the resistance forces [7]. A numerical calculation of $M_\phi(\phi)$ made for the initial conditions: pressure $p_+ = 70$ kg/cm^2 (hydrogen), $I = 0.82 \cdot 10^{-6}$ kg·cm·sec^2, $M = 0$, and $f_+ = f_-$, indicated (Fig. 2) that this function can be approximated quite well by the linear relation (dashed line)

$$M_\varphi = M_1 - (M_1 - M_2)\frac{2\varphi}{\pi}, \quad \left[M_1 = M_\varphi(\varphi = 0),\ M_2 = M_\varphi\left(\varphi = \frac{1}{2}\pi\right)\right] \tag{1.3}$$

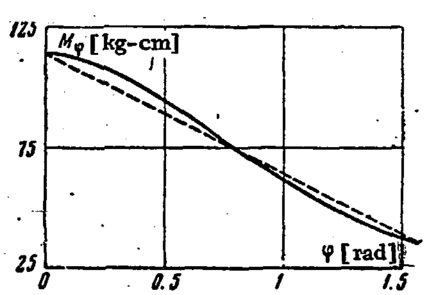

Figure 2

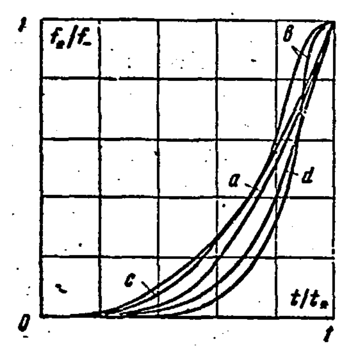

Figure 3

Here M_1 and M_2 can be determined in advance, since, according to the flow model adopted, the flow variables in sections z and * ($x \sim 0$) agree at time zero ($\phi = 0$) and when the diaphragm is wide open ($\phi = \frac{1}{2}\pi$) with the corresponding variables in section $x = 0$, which can be determined from the ideal model [1, 2]. Then, substituting (1.3) into (1.2) and assuming that $\dot{\phi}_0 = 0$ and $\phi_0 = 0$ at $t_0 = 0$, we obtain

$$t = \left[\frac{2\pi J}{M_1 - M_2}\right]^{1/2} \arcsin\left[\frac{M_1 - M_2}{M_1}\frac{\varphi}{\pi}\right]^{1/2} \tag{1.4}$$

Solving (1.4) and (1.2) simultaneously on the assumption of constant ratio of specific heats γf, we obtain the function $f^* = f^*(t)$ in the form

$$\frac{f_*}{f_-} = 2\sin^2\left\{\frac{1/2\pi}{E(\gamma)}\sin^2\left[\frac{t}{t_*}\arcsin\left(\frac{E(\gamma)}{2}\right)^{1/2}\right]\right\}, \quad E(\gamma) = 1 - \left(\frac{2}{\gamma_+ + 1}\right)^\Gamma \quad \left(\Gamma = \frac{2\gamma_+}{\gamma_+ - 1}\right) \tag{1.5}$$

Figure 3 compares our relationship (1.5) (line a) with those found experimentally in [8] (line b), [9] (line c), and [5] (line d). We see that Formula (1.5) describes the diaphragm opening curve quite satisfactorily, and it will be used in the calculations to follow.

The total diaphragm opening time t* can be found if we set $\phi = \frac{1}{2}\pi$ in (1.4). Thus, for a diaphragm of thickness δ made from a material with a density ρ and inserted in a square-section ($H \times H$) shock tube (with scoring along the diagonals of the square), we have

$$t^* = N\left(\frac{\rho H\delta}{p_+}\right)^{1/2} \qquad N = \left[\frac{1/2\pi}{E(\gamma)}\right]^{1/2} \arcsin \left[\frac{E(\gamma)}{2}\right]^{1/2} \tag{1.6}$$

We note that (1.6) was derived in [10] by dimensional analysis based on the results of [7], where it was shown that inertial forces are decisive for diaphragm opening. As we see from (1.6), N is determined by the nature of the gas; N = 0.9506 for $\gamma_+ = 1.4$.

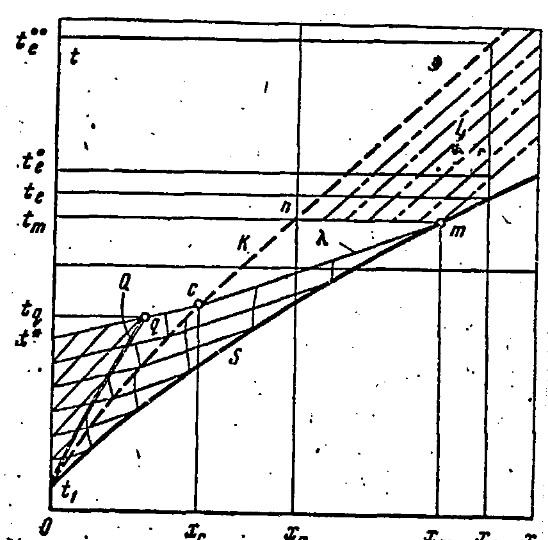

Figure 4

Equation (1.6) can also be used for approximate determination of t* in a round-section shock tube, for which $d\sqrt{2}$ must be substituted for H. /122

The values of $t^* = t_1^*$ (in μsec) computed by (1.6) are in satisfactory agreement with the measured $t^* = t_2^*$ for various t_+ (in kg/cm²), geometrical dimensions H and δ (in cm) and diaphragm materials (literature sources are indicated in the last column of Table 1). The experimental values of t_2^* given in [8] are an exception.

2. The flow variables and the variations of shock-wave propagation velocity on the acceleration segment of the shock tube (below section z) were computed on an M-20 electronic digital computer by the method of characteristics [14, 15], using the dimensionless parameters

$$T = \frac{t}{t^*}, \quad X = \frac{x}{a_{\pm}t^*}, \quad P = \frac{p}{p_+}, \quad U = \frac{u}{a_+}, \quad V = \frac{v}{a_+}, \quad A = \frac{a}{a_+} \tag{2.1}$$

Here x is distance, a is the speed of sound, u is velocity, and v is shock-wave velocity. It was assumed, as in [7], that the gases are inviscid and nonheat-conducting, have constant ratios of specific heats, and are intermiscible.

When the variables of (2.1) are used in the calculations, the starting initial parameters of the present problem will be, as in calculation of the flow variables from the ideal model, $P_- = p_- / p_+, A_- = a_- / a_+, \gamma_-, \gamma_+$.

TABLE 1

p_+	H	Diaphragm	δ	t_1^*	t_2^*	
15÷30	4.03	Steel	0.0254÷÷0.0889	310÷580	600	[3]
17.5	1.343	Al	0.02286	94	180	[8]
25.9	1.343	Al	0.03302	92	180	
10.2	2.695	Cu	0.0254	343	1050	
9.46	2.5	Brass	0.055	475	520	[9]
26	2.5	Brass	0.055	287	344	
56.8	2.5	Brass	0.055	193	163	
1.41	0.0898	Al	0.0254	88	85÷105	[11]
1.34	0.0898	Al	0.0254	90	105÷145	
15	2.24	Al	0.00254	42	45	[12]
15	2.24	Al	0.0108	84	105	
3.5÷5.6	15.3	Al	0.0508	854÷1030	1000	[13]

The calculations were carried out for the following initial-parameter values:

a) $\gamma_- = \gamma_+ = 1.67, \quad A_- = 1, \quad P_- = 0.5 \cdot 10^{-1} \div 0.5 \cdot 10^{-7}$ (set 1)
b) $\gamma_- = \gamma_+ = 1.4, \quad A_- = 1, \quad P_- = 0.5 \cdot 10^{-1} \div 0.5 \cdot 10^{-10}$ (set 2)
c) $\gamma_- = 1.4, \quad \gamma_+ = 1.67, \quad A_- = 0.3428, \quad P_- = 0.5 \cdot 10^{-1} \div 0.5 \cdot 10^{-8}$ (set 3)
d) $\gamma_- = \gamma_+ = 1.4, \quad A_- = 0.26263, \quad P_- = 0.5 \cdot 10^{-1} \div 0.5 \cdot 10^{-10}$ (set 4)

The calculated results to be given below for these initial-parameter values will be designated for brevity as Sets 1, 2, 3, and 4, respectively. /123

The computed family of characteristics appears in Fig. 4 (the flow diagram is in Fig. 1), where the solid line S is the shock wave, the dashed line K is the contact surface, the double light line Q is the disturbance that arises in the driving gas, the solid light lines λ are the characteristics, and the dot-dash lines L are particle trajectories. The initial system of waves at time t_1 (near t = 0) was determined from solution of an arbitrary-discontinuity decay problem whose initial conditions were the parameters of the driven gas at t = 0 and those of the driving gas in section z at t_1. We note that as t_1 is

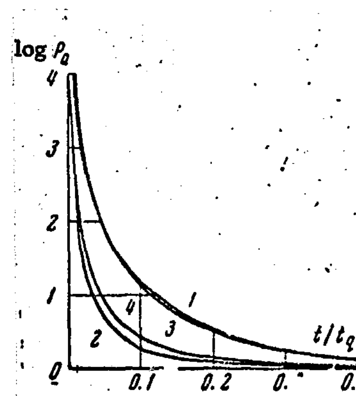

Figure 5

varied from t* to t = 0, the disturbance Q (Fig. 4) will at first be a decompression wave and then a shock wave, with the intensity of this wave increasing with decreasing t_1. Thus the disturbance Q was always a shock wave when the calculations were made in the initial wave system.

The presence of the shock wave Q during the initial phase of diaphragm opening was observed experimentally in [16]. With time, the shock wave Q degenerates into an acoustic wave. The rapid decrease in the intensity of shock wave Q with time t/t_q (t_q is the ordinate of the point at which the last characteristic originating from the point with the coordinates x = 0, t = t* meets the shock wave Q (Fig. 4)) is evident from Fig. 5, where we have plotted curves of the pressure ratio P_q across this wave for Sets 1, 2, 3, and 4 with $P_- = 0.5 \cdot 10^{-7}$.

The calculations were broken off after the last characteristic met shock wave S (point M, Fig. 4), for the following reasons. Owing to the rapid decay of shock wave Q, the region of driving-gas flow parameters above this characteristic represents, except for a narrow strip near the contact surface (which we shall not take into consideration in the subsequent discussion), an isentropic flow, which, since it is contiguous with the constant-parameter flow in section z, is a simple wave [17]. After passage of this wave, therefore, there will be no characteristic of additional disturbances to the motion of the shock wave from this region. Thereafter, the variation of particle velocity and pressure along the last characteristic in the driven gas did not exceed one percent in any of the cases computed, although the speed of sound varied considerably. In view of this practical absence of velocity and flow-pressure gradients, it can be stated that there will not be any appreciable pressure and velocity disturbances above the last characteristic in this region as well. This is consistent with the exact solution of the one-dimensional nonsteady flow equations in the form

$$p = \text{const}, \quad u = \text{const}, \quad \frac{\partial S}{\partial t} + u\frac{\partial S}{\partial x} = 0 \quad \left(\frac{\partial \rho}{\partial t} + u\frac{\partial \rho}{\partial x} = 0\right)$$
$$\rho = \rho(x - ut), \qquad a = a(x - ut)$$

Figure 6, a, b, c, and d, presents curves of v/v_m as a function of x/x_m for the indicated gradients P_- and Sets 1, 2, 3, and 4, respectively. Here and below, v_m is the velocity of shock wave S at point M (x_m, t_m), at which the last characteristic meets this wave. Figure 7 shows X_m and T_m as functions of the initial gradient P_- for these sets of conditions; here, the curve numbers match the set numbers. With (1.6), the diagrams of Figs. 6 and 7 easily yield the velocity change of shock wave S on the

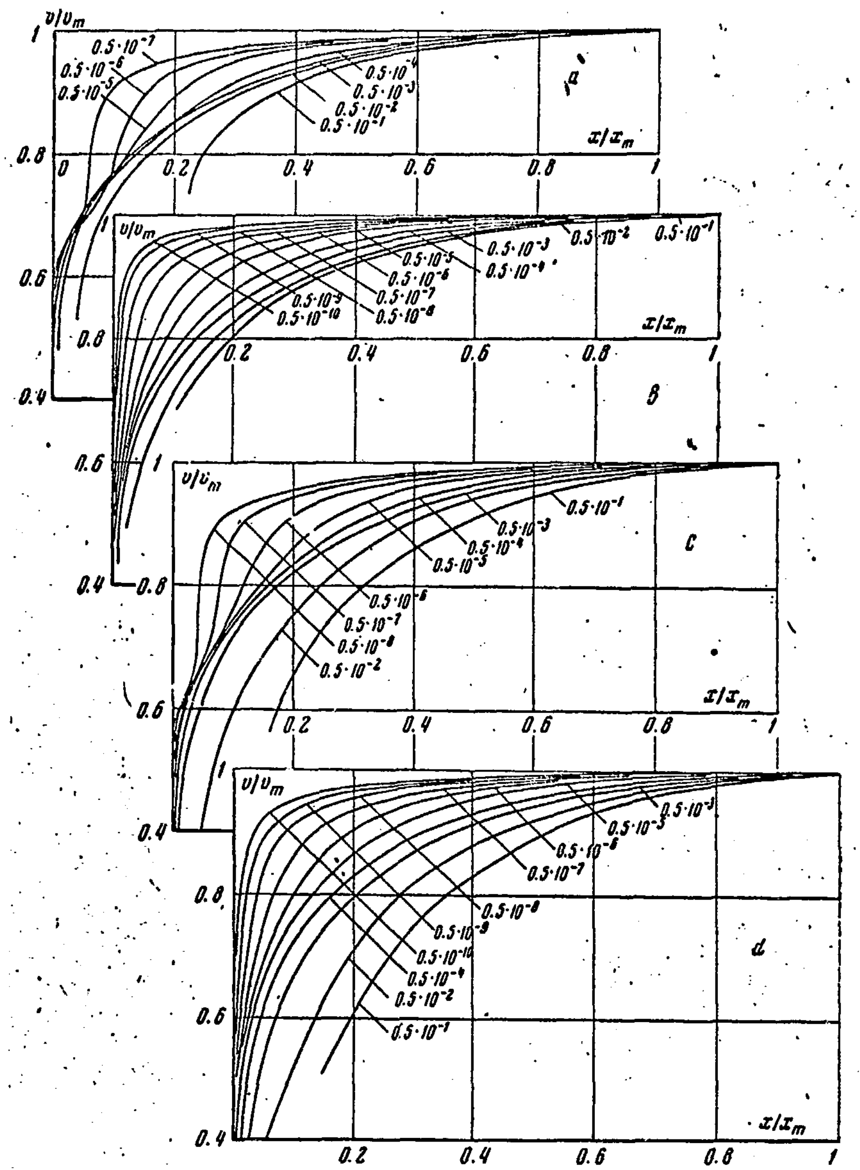

Figure 6

accelerating segment for each specific combination of gas initial variables, tube geometrical dimensions, and diaphragm material. It is interesting to note that a characteristic inflection of the curves, which increases with diminishing P_-, appears in Fig. 6, a c for $\gamma_+ = 1.67$. Supplementary calculations indicated that, other conditions the same, this inflection increases with increasing γ_+ despite the fact that the manner in which the variables change in section z, which determines the downstream flow, undergoes no marked disturbances.

As we have already noted, the absence of appreciable changes in flow velocity and pressure along the last characteristic in the driven gas guarantees the absence of marked pressure and velocity disturbances and, consequently, preservation of variables such as the speed of sound, entropy, and density along the trajectories of particles moving at constant velocity u_m in the region above the last characteristic.

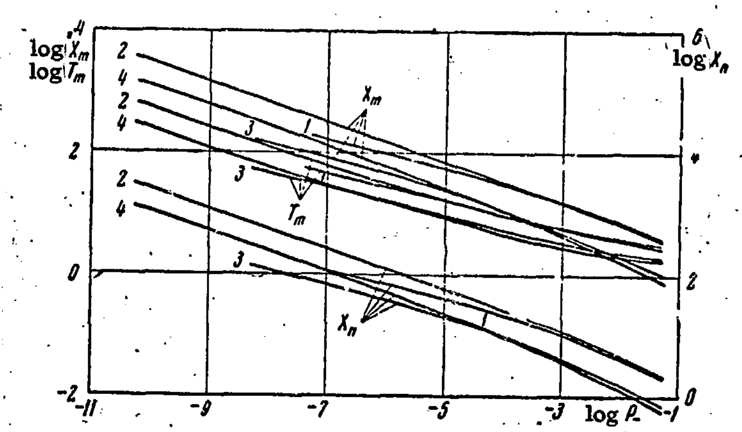

Figure 7

This makes it possible to carry the values of a obtained on the last characteristic along these trajectories to determine the influence of noninstantaneous diaphragm opening on the working-plug parameters after the shock wave has passed through the accelerating segment. Figure 8, a, b, c, and d, presents values of a/a_m as a function of $\eta = (x - x_n)/(x_m - x_n)$ for Sets 1, 2, 3, and 4, respectively. Here, x_n is the abscissa of the intersection point of the contact surface with the line t_m = const, and a_m is the speed of sound on shock wave S at point m. Figure 7 shows X_n as a function of P_- for the sets of conditions for which the computations were made. Figure 8 shows that after acceleration of the shock wave, the driven gas has substantial sonic-velocity nonuniformities, and hence also temperature, density, and other nonuniformities stemming from the prior history of shock-wave motion. Qualitatively similar results were obtained in [6]. /124

Figure 9, which typifies the sets of conditions computed, presents curves of the driving-gas variables a/a_k, u/u_k, p/p_k (the subscript k indicates the parameters of the driving gas at point c, Fig. 4) as they vary along the last characteristic for Set 2 with $P_- = 0.5 \cdot 10^{-5}$ (the dot-dash line indicates the position of the disturbance Q, which is in this case an analog of the decompression-wave tail in the ideal model); from them, we can infer the absence of the uniform driving-gas plug predicted by ideal theory toward the end of the shock-wave acceleration distance. As we should expect, the values obtained for v_m by the above method for Set 2 (the solid line in Fig. 10) lie between the /126 values computed with the White model (dashed line) and the ideal model (v_τ).

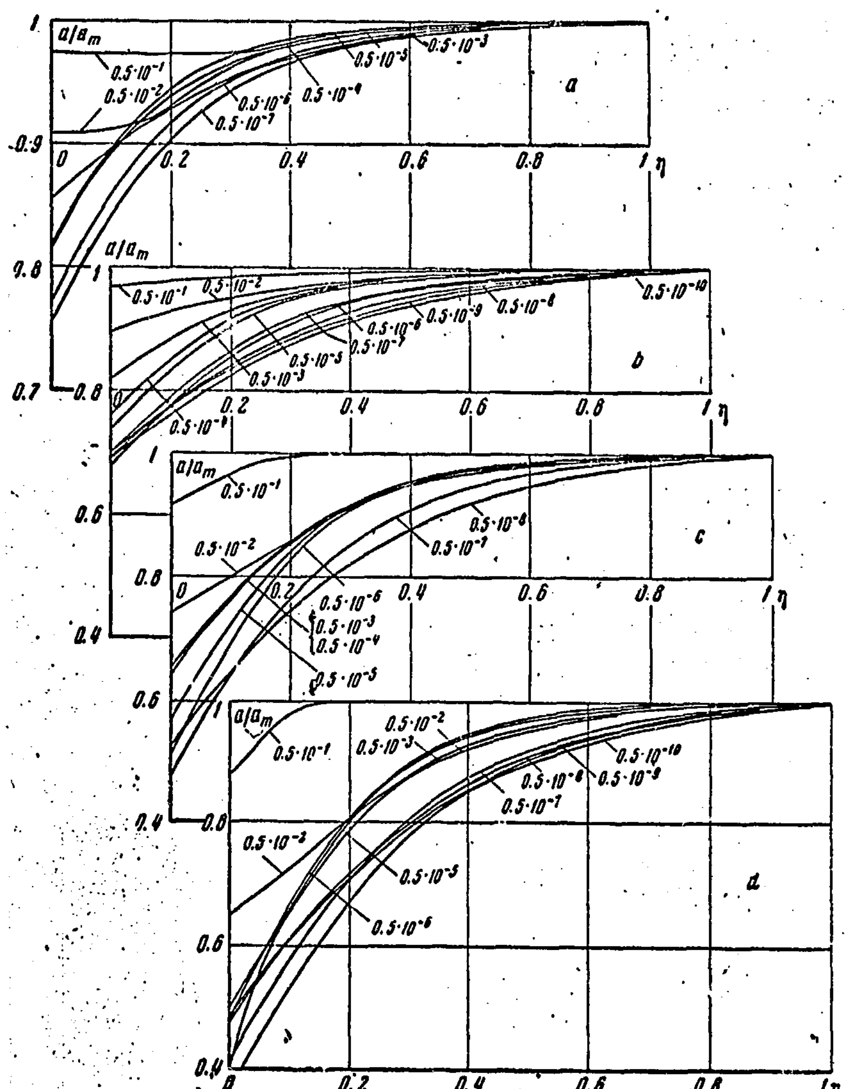

Figure 8 /125

The calculations given above took account of the driving-gas total-pressure losses only in the shock wave Q. However, it may be necessary to consider impact losses at small relative diaphragm apertures when these losses are substantially larger than those in the normal shock. With this in mind, a calculation was made on the scheme of Fig. 1, where, as before, the flow rate and energy conservation equations were written between sections 1, *, and z, and the condition of constant entropy between sections * and z was dropped; the flow in section z then became subsonic, and the disturbances propagated upstream arrived at section *. Below section z, the flow was, as before, assumed to be one-dimensional

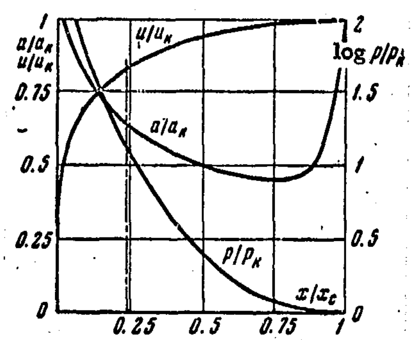

Figure 9

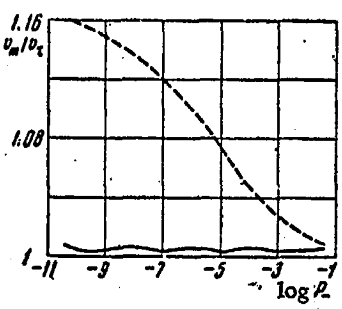

Figure 10

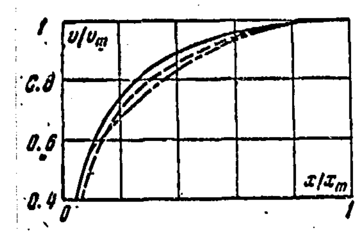

Figure 11

and nonsteady. Comparison of the variation of v/v_m down the length of the low-pressure chamber as computed with consideration of the above condition (dashed line in Fig. 11) and that determined from Fig. 6 (solid line) with the experimental curves [5] (dot-dash line) indicates good agreement of the computed results with the experimental data. The agreement of the calculated results (Fig. 11) obtained with the above assumptions is obviously due to the fact that the contribution of the flow-variable change to acceleration of the shock wave is small at small diaphragm apertures (when a substantial difference is observed in the total-pressure losses) by comparison with the contribution made at relatively large diaphragm apertures (when the difference in the total-pressure losses practically vanishes).

TABLE 2

$H_2 - N_3$

p_+	p_-	ξ_1	[illegible]
212	5	0.7	0.62
200	5	0.7	0.65
198	10	0.794	0.73
102	10	0.72	0.61
120	10	0.72	0.66
114	50	0.8	0.7

3 We present a comparison of the experimentally measured density profile behind the shock wave in the driven gas with that determined from the curves of Fig. 8 and Eq. (1.6). The experimental variation of the density profile in the gas flow behind the shock wave was determined from oscillograms obtained by the photoelectric shadow method [18] and representing the time distribution of the refractive-index gradient of the gas

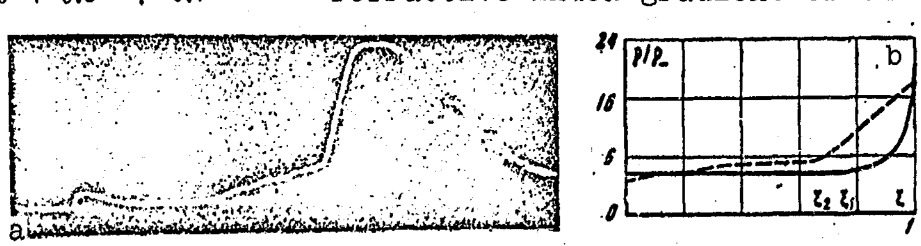

Figure 12

flow studied. The measurements were made in a shock tube 50 mm in inside diameter at a distance of 8 m from the diaphragm. One of the oscillograms appears in Fig. 12a. It shows the characteristic inflection of the trace in the zone between the two spikes, corresponding to passage of the shock wave and the contact region. The variation of the density ρ/ρ_- (ρ_- is the initial density of the driven gas) determined for the driven gas from this oscillogram (dashed line) is compared in Fig. 12b with the calculated change (solid line). Table 2 gives calculated (ξ_1) and experimentally measured (ξ_2) values of $\xi = (t_e^\circ - t_e)/(t_e^\infty - t_e)$. Here, t_e^∞ and t_e (Fig. 4) are the times of passage of the contact surface and shock wave across the measurement cross section (x_e) and t_e° is the time of passage of the boundary of the zone disturbed by diaphragm opening across the section of measurement. The table also gives the initial variables of the gases (p_+ in kg/cm^2 and p_- in mm Hg) in the shock-tube chambers. Comparison of the experimental data with the computed data in Table 2 and Fig. 12 indicates that the density profile observed experimentally in the driven gas behind the shock wave can be explained as due to noninstantaneous diaphragm opening. /127

The authors thank Yu.A. Dem'yanov, G.I. Taganov, and T.V. Bazhenova for their helpful discussion of this work.

Received August 2, 1968

REFERENCES

1. Glass, I. and Patterson, G. Theoretical and experimental study of shock-tube flows, in collection entitled "Udarnyye truby" (Shock Tubes), Moscow, Izd-vo inostr. lit., 1962, pages 138-189.
2. Khenshell, B. Certain aspects of the use of shock tubes in aerodynamic research, in collection entitled "Udarnyye truby," Moscow, Izd-vo inostr. lit., 1962, pages 2-137.
3. White, D.R. Influence of diaphragm opening time on shock-tube flows. J. Fluid. Mech., 1958, Vol. 4, No. 6, pages 585-599.
4. Bazhenova, T.V., Naboko, I.M., and Predvoditeleva, O.A. Influence of dissipation on flow variables behind the shock in a shock tube, in collection entitled "Fizicheskaya gazodinamika i svoystva gazov pri vysokoy temperature" (Physical gasdynamics and the properties of gases at high temperature), Moscow, "Nauka," 1964, pages 80-91.
5. Shtemenko, L.S. Gas flow near the diaphragm in a shock tube, Vest. Mosk. un-ta, ser. Fizika, astronomiya, 1967, No. 1, pages 58-64.
6. Busygin, E.P. and Tumakayev, G.K. Measurement of gas density behind the shock wave in a shock tube by the electron-beam method, Zh. tekhn. fiz., 1964, Vol. 34, No. 1, page 122.

7. Kireyev, V.T. Shock-wave motion for noninstantaneous opening of shock wave [sic] diaphragm, Izv. AN SSSR, OTN, Mekhanika i mashinostroyeniye, 1962, No. 6, pages 144-146.
8. Campbell, G.A., Kimber, G.M. and Napier, D.H. Bursting of diaphragms as related to the operation of shock tubes, J. Sci. Instrum., 1965, Vol. 42, No. 6, pages 381-384.
9. Simpson, C.Y.S.M., Chandler, T.R.D., and Bridgman, K.B. Effect on shock trajectory of the opening time of diaphragms in a shock tube, Phys. Fluids, 1967, Vol. 10, No. 9, Part 1, pages 1894-1896.
10. Spense, D.A. and Woods, B.A. A review of theoretical treatments of shock tube attenuation, J. Fluid Mech., 1964, Vol. 19, No. 2, pages 161-174.
11. Bradley, Y.N., Bytlin, R.N. and Quinn, Y.G. An electrical method for breaking shock tube diaphragms, J. Sci. Instrum., 1965, Vol. 42, No. 12, page 901.
12. Coates, P.B. and Gaydon, A.G. A simple shock tube with detonating driver gas, Proc. Roy.Soc., Ser. A, 1965, Vol. 283, No. 1392, pages 18-32.
13. Roshko, A. and Baganoff, D. A novel device for bursting shock-tube diaphragms, Phys. Fluids, 1961, Vol. 4, No. 11, pages 1445-1446.
14. Zhukov, A.I. Use of the method of characteristics for numerical solution of one-dimensional problems in gas dynamics, Tr. Matem. in-ta AN SSSR, 1960, No. 58.
15. Volkonskaya, T.G., Pavlov, B.M., and Popov, N.N. Calculation of compression process in piston machines, in collection entitled "Chislennyye metody v gazovoy dinamike" (Numerical methods in gasdynamics), No. 4, Izd-vo MGU, 1965, pages 184-210.
16. Shtemenko, L.S. Formation of compression shock during initial phase of gas flow near a shock-tube diaphragm, Vestn. Mosk. un-ta, ser. Fizika, astronomiya, 1968, No. 3, pages 82-87. /128
17. Kurant, F. and Fridrikhs, K. Sverkhzvukovoye techeniye i udarnyye volny (Supersonic flow and shock waves), Moscow, Izd-vo inostr. lit., 1950.
18. Vasil'yev, L.A., Galanin, A.G., Yershov, I.V., and Suntsov, G.N. A photoelectric shadow method for study of nonstationary processes, Pribory i tekhnika eksperimenta, 1964, No. 3.

Translated for the National Aeronautics and Space Administration by Scripta Technica, Inc. NASW-2036.